On the direct identification of propagation modes for HF plasma waves

Michel Parrot, François Lefeuvre, Y. Marouan

On the Direct Identification of Propagation Modes for HF Plasma Waves

M. Parrot, F. Lefeuvre, and Y. Marouan

Laboratoire de Physique et Chimie de l'Environnement, Centre National de la Recherche Scientifique
Orléans, France

We examine the problem of interpreting the direct measurement of the polarization sense for HF plasma waves, in a cold and collisionless magnetoplasma when two propagation modes are simultaneously present. Two types of propagation mode estimators are considered. The first, generally more sensitive to quasi-parallel waves, consists in the determination of the signs of cross-spectra between two electric or two magnetic wave field components, both perpendicular to each other and to B_0. The second, more sensitive to quasi-perpendicular waves, is obtained by testing the ratio of the parallel to the perpendicular energy, against physical thresholds. Interpretations of the results are shown to be a function of the wave and plasma parameters. Applications performed on synthetic data constructed from two propagation mode models with different wave distribution functions (WDF) are presented. They show that the combination of the different propagation mode estimators often enables us to point out the presence of the two modes. Moreover, when the WDFs of the two modes are very different and when the wave frequency is far from the characteristic frequencies of the medium, the main propagation properties of each mode may be derived.

1. Introduction

The direct identification of the magnetoionic mode of high-latitude wave emissions is still controversial. As discussed by *Stix* [1962], cold-plasma theory predicts four distinct electromagnetic modes of propagation at frequencies above the ion gyrofrequency. These modes are the free-space *L-O* mode (left-hand polarized, ordinary mode), the free-space *R-X* mode (right-hand polarized, extraordinary mode), the whistler mode, and the *Z* mode. With the exception of a few regions in the Clemmow-Mullaly-Allis (CMA) diagram, two modes may coexist [*Stix*, 1962; *Allis et al.*, 1963].

At present, the controversy is particularly strong as to the mode of auroral kilometric radiation (AKR). Because the radiation escapes freely from the Earth, it must be propagated in the free-space modes. Several polarization studies, mainly based on comparisons between the wave frequencies and the characteristic frequencies of the medium, conclude that the radiation is generated in the *R-X* mode [*Gurnett and Green*, 1978; *Kaiser et al.*, 1978; *Benson and Calvert*, 1979]. However, *Oya and Morioka* [1983] have presented evidence that radiation is propagated in the *L-O* mode. One explanation proposed by *Benson* [1984] is that the *R-X* mode emanates from low-density cavities above the auroral regions and that the *L-O* mode is dominant in regions of relatively high electron density. Direct polarization measurements performed on DE 1, using orthogonal dipole electric antennas oriented such that, from time to time, they become perpendicular to the local magnetic field vector B_0, have pointed out the presence of *R-X* modes [*Shawhan and Gurnett*, 1982]. The detection of the *L-O* mode in other regions is obviously not excluded. The point is that the identification of the AKR wave mode in satellite wave observations is important to the development of a correct theory for the AKR generation mechanism; for a review on AKR, see *Grabbe* [1981] and *Oya and Morioka* [1983].

As shown by *Lefeuvre et al.* [1986], the mode that is identified from electric or magnetic wave field component measurements is not always the one that conveys the maximum wave energy density. Suppose that the *L-O* and the *R-X* modes are simultaneously present in the wave observations presented by *Shawhan and Gurnett* [1982]. As the *R-X* mode gives the sense of polarization, one may be led to conclude that the *R-X* mode conveys the most energy. However, this may not be the case. According to *Lefeuvre et al.* [1986], the kind of estimators used by Shawhan and Gurnett, first, may be strongly biased in the vicinity of the critical frequencies, and so probably around the electron gyrofrequency where the AKR is supposed to be generated [*de Feraudy et al.*, 1987], and, second, may favor the mode corresponding to waves having the wave normal direction K along the Earth's magnetic field B_0. Then, before interpreting polarization measurements, it is indispensable to evaluate the possible bias of the estimators and to find a way to check whether oblique waves propagating in the *L-O* mode are simultaneously present with the *R-X* mode or not.

The aim of the present paper is to give a general approach allowing us to answer these requirements. No hypothesis is made, a priori, about the distribution of the angle θ between K and B_0. The study is not restricted to AKR phenomena but is extended to all HF waves, i.e., to all waves with frequencies well above the proton gyrofrequency. The medium is supposed to be a cold collisionless magnetoplasma. In the absence of satellite data with more than three wave field components, we have tested our ideas on synthetic data only. But the methods described here will find full applications in future satellite missions such as Interball, where three magnetic wave field components and one electric field component will be transmitted to the ground in the HF range. Furthermore, they will be of prime importance in the design of future satellite missions when selecting which field components to measure and transmit to the ground.

The plan of the paper is as follows: Section 2 recaptures the dispersion relation and the characteristic frequencies of the medium. The wave distribution function (WDF) concept is used to evaluate the contribution to the sense of polarization, when different waves modes are simultaneously present. It is shown that two polarization estimators (for
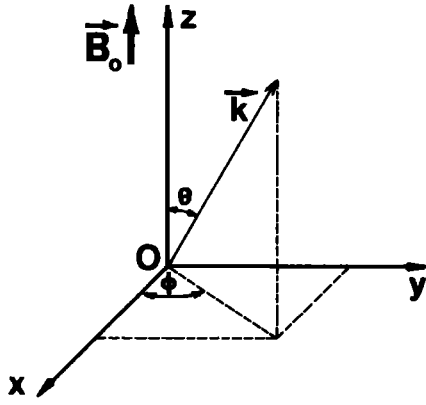
Fig. 1.   Cartesian coordinate system used in the paper.

quasi-parallel and quasi-perpendicular waves) can give the polarization mode in the general case where the θ distribution is unknown. Examples of synthetic data are given. The validity domains and thresholds needed to compare to experimental data are given in section 3. Section 4 offers some general conclusions.

2.   Estimators of the Polarization Sense

The Dispersion Relations

A Cartesian coordinate system $Oxyz$ (Figure 1) is assumed, in which the z axis lies along $\mathbf{B}_0$, the x axis is in the local magnetic meridian plane and points in the direction away from the Earth, and the y axis is oriented eastward. In this system, the wave normal direction $\mathbf{K}$ is characterized by the polar angle θ and the azimuthal angle ϕ, as measured from the local magnetic meridian plane. Considering variations of the electric and magnetic fields proportional to exp $i(2\pi ft - \mathbf{K} \cdot \mathbf{r})$, and taking $\phi = 0$, the dispersion relation is expressed as

$$\begin{pmatrix} S - n^2 \cos^2 \theta & iD & n^2 \cos \theta \sin \theta \\ -iD & S - n^2 & 0 \\ n^2 \cos \theta \sin \theta & 0 & P - n^2 \sin^2 \theta \end{pmatrix} \begin{pmatrix} E_x \\ E_y \\ E_z \end{pmatrix} = 0 \qquad (1)$$

where n is the refractive index ($n = kc/2\pi f$ with c the velocity of light). The quantities S, D, and P are defined as by Stix [1962], but for frequencies well above the proton gyrofrequency they can be written

$$S = \tfrac{1}{2}(R + L) \qquad D = \tfrac{1}{2}(R - L)$$

$$R \simeq 1 - \frac{f_{pe}^2}{f(f - f_{ce})} \qquad L \simeq 1 - \frac{f_{pe}^2}{f(f + f_{ce})}$$

$$P \simeq 1 - \frac{f_{pe}^2}{f^2}$$

where f_{ce} and f_{pe} are the electron gyrofrequency and plasma frequency.

The main types of electromagnetic plasma waves observed in high-latitude auroral regions are represented in the CMA diagram [Stix, 1962] in Figure 2. Since the wave frequency is high, the ion effect is negligible, and we do not consider regions above 8. The R-X mode is a fast extraordi-

nary mode, whose low-frequency cutoff is the $R = 0$ cutoff in the CMA diagram:

$$f_x = \sqrt{f_{pe}^2 + \left(\frac{f_{ce}}{2}\right)^2} + \frac{f_{ce}}{2} \qquad (2)$$

The low-frequency cutoff of the L-O mode is at the electron plasma frequency f_{pe}, i.e., $P = 0$ in the CMA diagram. The Z mode is a slow extraordinary mode bounded by the upper hybrid resonance ($S = 0$ in the CMA diagram):

$$f_{UHR} = \sqrt{f_{pe}^2 + f_{ce}^2} \qquad (3)$$

and the $L = 0$ cutoff:

$$f_Z = \sqrt{f_{pe}^2 + \left(\frac{f_{ce}}{2}\right)^2} - \frac{f_{ce}}{2} \qquad (4)$$

The Z mode radiation may be a right-hand ($f_{pe}/f < 1$) or a left-hand ($f_{pe}/f > 1$) polarized mode. The whistler mode is limited by either f_{pe} or f_{ce}, whichever is smaller. Other representations of auroral wave emission can be seen in Figure 2 of Gurnett et al. [1983] and in Figures 3 and 4 of Grabbe [1981]. From the CMA diagrams in Figure 2, it is seen that the R-X mode and the L-O mode can coexist, as well as the L-O mode and the Z right-handed mode, or the Z left-handed mode and the whistler mode.

The Use of the WDF Concept

Assuming that Oz is parallel to $\mathbf{B}_0$ (Figure 1), the electric and magnetic wave field components are combined for the sake of convenience in a generalized electric vector ε whose components are

$$\varepsilon_{1,2,3} = E_{x,y,z} \qquad \varepsilon_{4,5,6} = Z_0 H_{x,y,z} \qquad (5)$$

with Z_0 being the wave impedance in free space. The WDF specifies how the wave energy is distributed relative to the two angles θ and ϕ, the wave frequency f, and the propagation mode m (ordinary or extraordinary). It is written $F_m(f, \cos \theta, \phi)$ and defined as being everywhere nonnegative. [Storey and Lefeuvre, 1979]. At a given wave frequency f_0, it is related to the autospectra and cross-power spectra of the six wave field components by the expression

$$S_{ij}(f_0) = \frac{\pi}{2} \sum_m \oiint a_{ijm}(f_0, \cos \theta, \phi) F_m(f_0, \cos \theta, \phi) \, d\sigma \qquad (6)$$

The integral is taken over the surface of a unit sphere, where $d\sigma = d \cos \theta \, d\phi$ is the solid-angle element. S_{ij} is either the autospectrum ($i = j$) or the cross-spectrum ($i \neq j$) between the ε_i and ε_j components. The coefficients a_{ijm}, which are the kernels of the integral equations, are directly related to the corresponding autospectra and cross-spectra for an elementary plane wave in the magnetoionic mode m. Their algebraic expression, derived from the Maxwell equations, is given by Storey and Lefeuvre [1980]. They implicitly depend on the plasma parameters f_{pe} and f_{ce}. The kernels whose expressions are needed here are listed in the appendix.
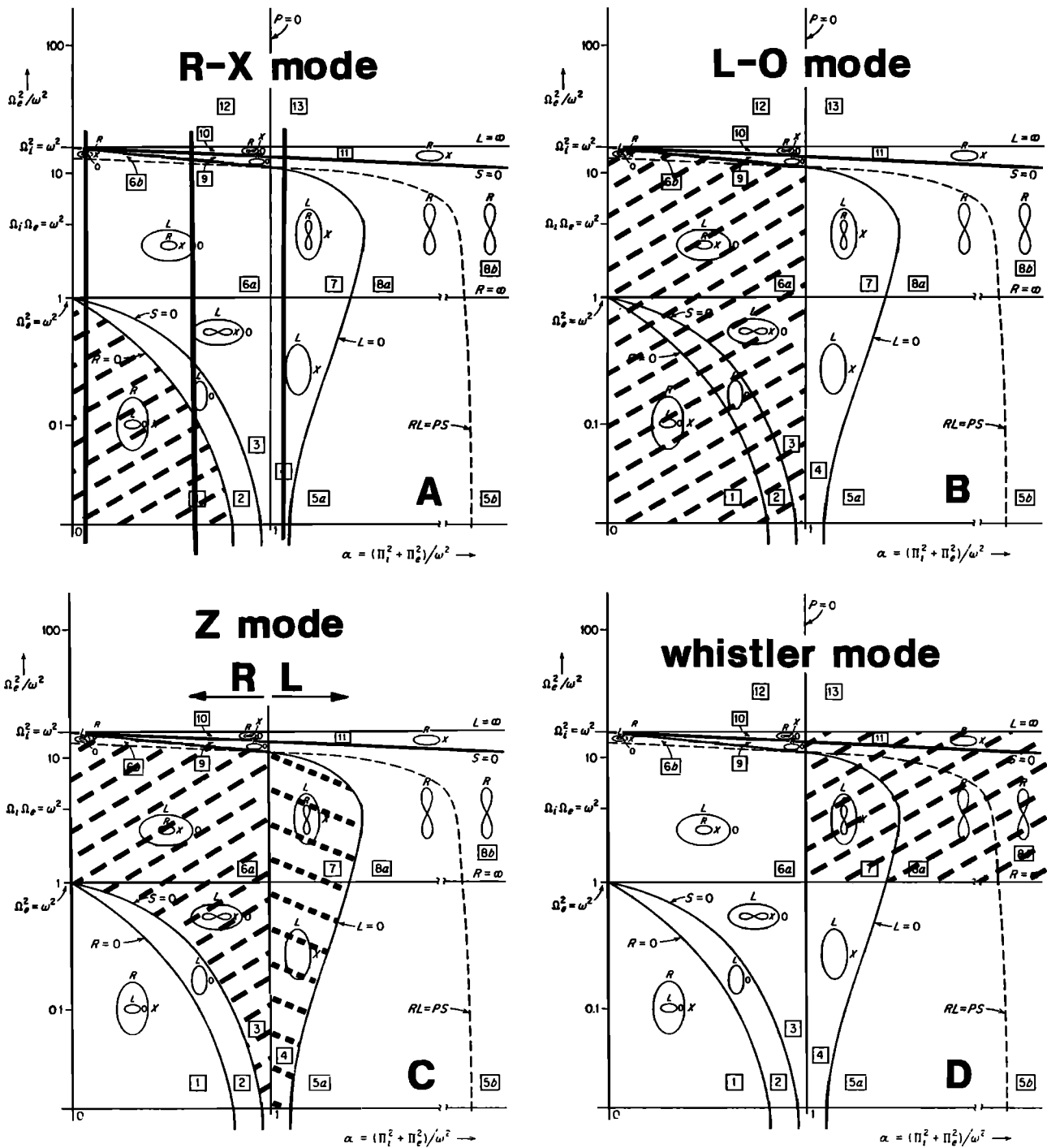
Fig. 2. CMA diagram from *Stix* [1962] with the main types of electromagnetic waves observed in the Earth's polar magnetosphere and with negligible ion effect. Hatched areas represent (a) the R-X mode; (b) the L-O mode; (c) the Z mode with right-hand polarization on the left of $f = f_{pe}$ and left-hand polarization on the right of $f = f_{pe}$; and (d) the whistler mode.

Polarization Estimator for Quasi-Parallel Waves

Lefeuvre et al. [1986] pointed out that for quasi-parallel waves, the signs of Im (a_{12m}) and $(n^2 - S)/D$ are the same in most regions of the CMA diagram: positive for right-handed and negative for left-handed waves. However, in a few regions the situation is more complicated, as shown by *Allis et al.* [1963]. In the regions denoted 3 and 10 by *Stix* [1962]

(5 and 11 by Allis et al.), the quantity $(n^2 - S)/D$ has the same sign for the two magnetoionic modes. This means that in those regions it is impossible to identify the propagation mode of a wave field from the cross-power spectral measurements of two electric components taken in a plane perpendicular to B_0. In regions denoted 6-a and 12 by Stix (13 and 7-a by Allis et al.), the situation is even more complicated. Here, the quantity $(n^2 - S)$ takes a zero value for a critical
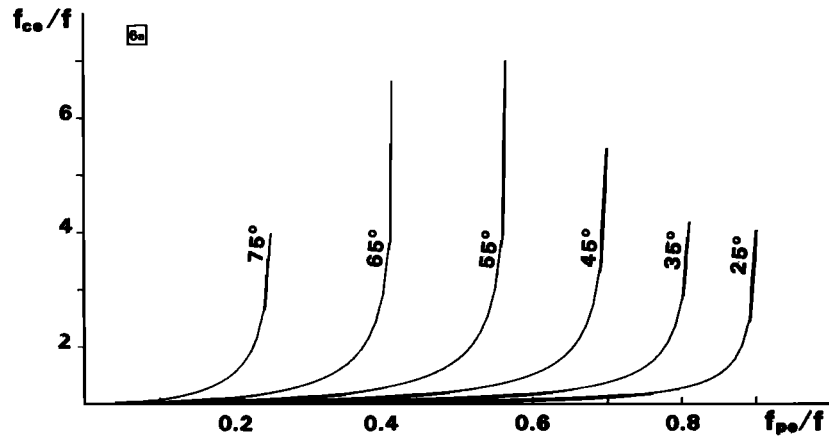
Fig. 3. Representation of $n^2 = S$ in region 6-a of the CMA diagram (Stix) for different θ_c values. When $f_{ce}/f \gg 1$ the asymptotic solution is given by $\cos \theta = f_{pe}/f$.

angle θ_c, given by $\sin^2 \theta_c = P/S$. Examples of θ_c values in region 6-a of the Stix diagram are displayed in Figure 3. For $n^2 < S$ to the right of the figure, it is impossible to identify the mode because the signs for the two modes are identical, while for $n^2 > S$ to the left, the R mode as well as the L mode can be distinguished. With the exception of the regions mentioned above, we obtain the relations for the cross-power spectra of the two components of the electric field orthogonal to $\mathbf{B}_0$:

$$\text{Im } (S_{12}) > 0 \leftrightarrow R \text{ waves}$$

$$\text{Im } (S_{12}) < 0 \leftrightarrow L \text{ waves} \tag{7}$$

A null value is associated either with a linear polarization or with an equal contribution of the L and R waves to the sign of Im (S_{12}).

The sign of Im (a_{45m}) also characterizes the polarization of quasi-parallel waves. It is the same as the sign of the quantity $(n^2 - S)P/[D(P - n^2 \sin^2 \theta)]$. Substituting for Im (a_{45m}) in (6), we get the relations for the cross-power spectra of the two components of the magnetic field orthogonal to $\mathbf{B}_0$:

$$\text{Im } (S_{45}) > 0 \leftrightarrow R \text{ waves}$$

$$\text{Im } (S_{45}) < 0 \leftrightarrow L \text{ waves} \tag{8}$$

which are independent of θ [Marouan, 1988] and valid in all regions of the CMA diagram without any restriction. A null value is associated either with a linear polarization or with an equal contribution of the L and R waves to the sign of Im (S_{45}).

One may evaluate the contribution of each mode to the sign of Im (S_{12}) and Im (S_{45}) by plotting Im (a_{12m}) and Im (a_{45m}) versus θ. One example was given in Figure 2 of Lefeuvre et al. [1986], and further examples are presented in Figure 4 for a range of plasma parameters. It can be observed that the estimators generally are more sensitive to small θ values. In region 1 of the CMA diagram (Figure 4: panels A_1, A_3, B_1, and B_3), electric as well as magnetic components can be used to determine the sense of polarization. For the case shown in Figure 4, panels A_1 and B_1, the contributions of the R and L modes are approximately the same with a slight tendency to enhance the L mode. Unless

a very intense wave energy density is conveyed at large θ waves, the sign of Im (a_{12}) and Im (a_{45}) is controlled by small θ waves. The reader will note that in the R mode the Im (a_{12m}) coefficient is not null at $\theta = 90°$, which means that large θ waves may contribute to the sign of Im (S_{12}).

For the case shown in panels A_3 and B_3, the variation with θ is completely different for the electric and the magnetic components. When considering first the magnetic ones, it can be seen that a large scale factor exists between Im (a_{45m}) in the L mode and in the R mode. The L mode is clearly dominant, with the consequence that unless the wave energy density in the L mode is negligible relative to the wave energy density in the R mode, it is the L mode only that contributes to the sign of Im (S_{45}). In other words, it is practically impossible to detect the presence of the R mode when the two modes coexist. As far as the electric measurements are concerned, the main point is the nearly constant value of Im (a_{12m}) in the R modes. At small θ values the L mode is dominant, but as soon as $\theta > 30°$, only the R waves contribute to the sign of Im (S_{12}), and it becomes impossible to use the sign of Im (S_{12}) as an estimator of the sense of polarization for quasi-parallel waves.

The variations of Im (a_{45m}) in region 3 of the CMA diagram are illustrated in Figure 4, panel B_4. At smaller θ values the R mode is limited by resonance angle. Since Im (a_{12m}) cannot be used as an estimator in this region, as mentioned above, it has not been shown.

Two examples are given for region 6-a of the CMA diagram in Figure 4, panels B_2 and B_5. Once more, only the magnetic estimator can be used. For the case of a low plasma frequency, shown in panel B_2, a slight tendency exists to enhance the L mode, whereas for the case of a higher plasma frequency, shown in panel B_5, the L mode has clearly the more important contribution to the sign of Im (S_{45}), at least for θ values less than 50°. The reader will note that the maximum contribution of the R waves is at $\theta = 30°$ and not at $\theta = 0°$.

Polarization Estimators for Quasi-Perpendicular Waves

Intuitively the polarization sense for perpendicular waves may be estimated from the quantities
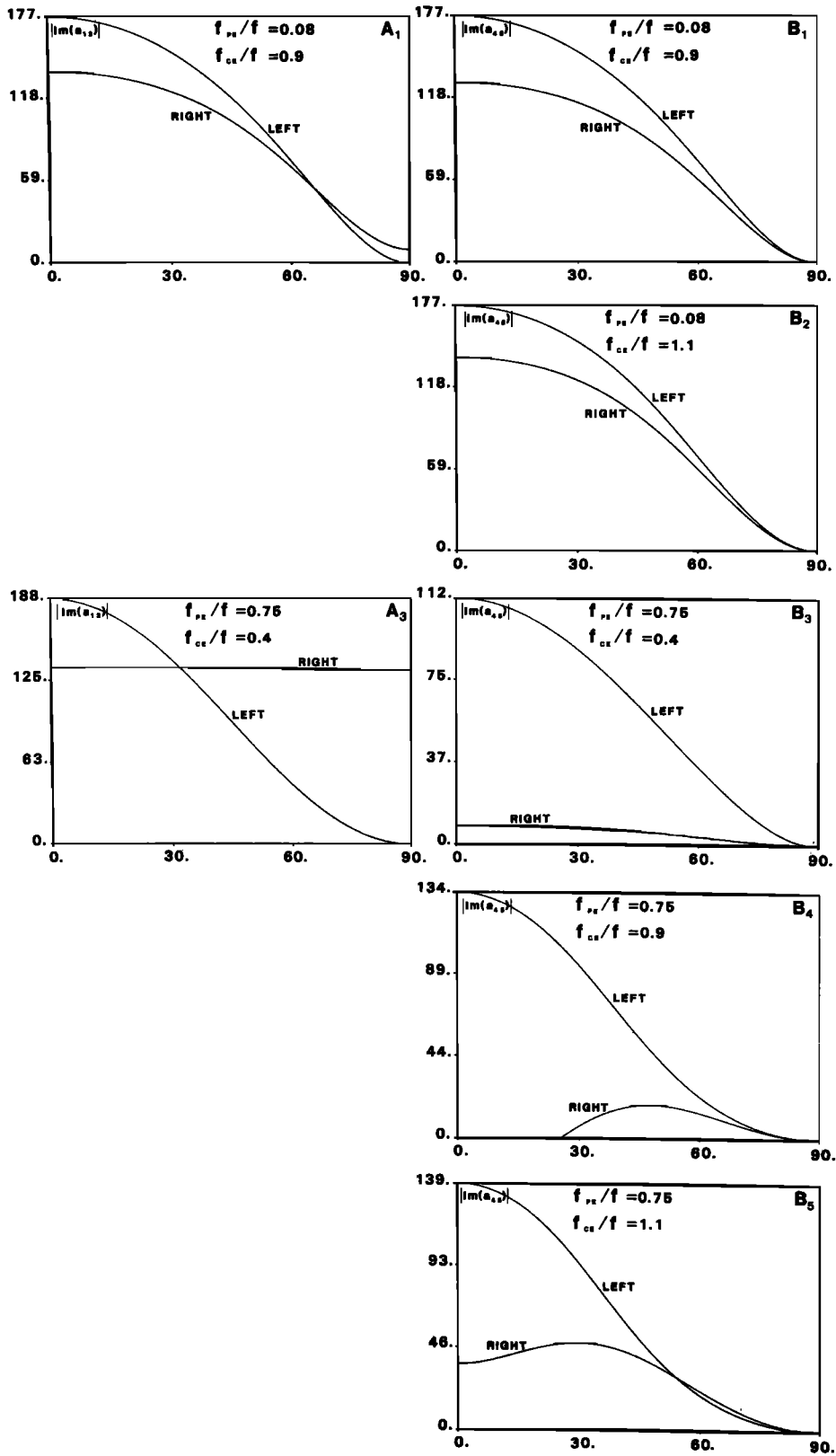
Fig. 4. Variations of the absolute values of Im (a_{12}) and Im (a_{45}) versus θ. The wave frequency is f = 300 kHz. We have (A$_1$ and B$_1$) f_{pe}/f = 0.08 and f_{ce}/f = 0.9, (B$_2$) f_{pe}/f = 0.08 and f_{ce}/f = 1.1, (A$_3$ and B$_3$) f_{pe}/f = 0.75 and f_{ce}/f = 0.4, (B$_4$) f_{pe}/f = 0.75 and f_{ce}/f = 0.9, and (B$_5$) f_{pe}/f = 0.75 and f_{ce}/f = 1.1. In each panel, right-hand polarization and left-hand polarization are considered. The units are arbitrary.

TABLE 1. Expressions of the Kernels of the Appendix in Special Cases

θ	n^2	Im (a_{12})	Im (a_{45})	a_{33}	$a_{11} + a_{22}$	a_{66}	$a_{44} + a_{55}$
0°	R	$\alpha/R^2\nu_R$	$\alpha/R\nu_R$	0	$2\alpha/\nu_R R^2$	0	$2\alpha/\nu_R R$
0°	L	$-\alpha/L^2\nu_L$	$\alpha/L\nu_L$	0	$2\alpha/\nu_L L^2$	0	$2\alpha/\nu_L L$
90°	P	0	0	$2\alpha/\nu_O P$	0	0	$2\alpha/\nu_O P$
90°	RL/S	$\dfrac{\alpha}{2\nu_X}\left(\dfrac{1}{R^2} - \dfrac{1}{L^2}\right)$	0	0	$\dfrac{\alpha}{\nu_X}\left(\dfrac{1}{R^2} + \dfrac{1}{L^2}\right)$	$2\dfrac{\alpha}{\nu_X}\dfrac{S}{RL}$	0

Here $\alpha = 1/\varepsilon_0$ and $\nu_i = 1/2 \, \omega^3 \, \{\partial/\partial\omega \, [- (\omega n)^{-2}]\}_i$; $i = R, L, O$ or X.

$$P_E = \frac{S_{33}}{S_{11} + S_{22}}$$

$$P_H = \frac{S_{66}}{S_{44} + S_{55}} \tag{9}$$

which represent the ratios of the parallel to the perpendicular energy for the electric and magnetic wave fields. For $\theta \rightarrow \pi/2$, $P_E \rightarrow \infty$ and $P_H \rightarrow 0$ for O polarization ($n^2 \rightarrow P$), whereas $P_E \rightarrow 0$ and $P_H \rightarrow \infty$ for X polarization ($n^2 \rightarrow RL/S$). In the following we will show that there are thresholds in P_E and P_H in certain cases allowing the identification of both the O and the X modes.

Consider first the following quantities:

$$P'_E(\theta)_m = \frac{a_{33m}(\theta)}{a_{11m}(\theta) + a_{22m}(\theta)} \qquad m = O, X$$
$$\tag{10}$$

$$P'_H(\theta)_m = \frac{a_{66m}(\theta)}{a_{44m}(\theta) + a_{55m}(\theta)} \qquad m = O, X$$

Examples of the functions $P'(\theta)_m$ are shown in Figure 5 (solid lines) for the wave and plasma parameters corresponding to Figure 4. Their characteristics can be understood with the aid of the expressions for a_{ij} listed in Table 1, from which it follows that $P'_E(0)_X = P'_E(\pi/2)_X = 0$. With the exception of regions 3, 10, 6-a, and 12, discussed in the previous section, $P'_E(\theta)_X$ is bounded by a maximum value Q_E at $\theta = \theta_E$. Similarly for the magnetic components, $P'_H(0)_O = P'_H(\pi/2)_O = 0$. In all regions of the CMA diagram, $P'_H(\theta)_O$ is bounded by a maximum value Q_H at $\theta = \theta_H$. Formally, Q_E and Q_H can be expressed as

$$Q_E = \max [P'_E(\theta)_X] \qquad 0 \leq \theta \leq \pi/2$$
$$\tag{11}$$
$$Q_H = \max [P'_H(\theta)_O] \qquad 0 \leq \theta \leq \pi/2$$

For the electric component of the O mode we find that $P'_E(0)_O = 0$ and $P'_E(\pi/2)_O = \infty$. Since the wave normal surfaces never cross, it follows that $P'_E(\theta)_O > P'_E(\theta)_X$ for $0 \leq \theta \leq \pi/2$, again in all regions except the ones mentioned above. Similar arguments for the magnetic component of the X mode lead to $P'_H(\theta)_X > P'_H(\theta)_O$, which is valid in all regions.

A wave field may consist of both O mode and X mode. An example of the P values for a mixed wave field is shown with dotted lines in Figure 5. The field is composed of two WDFs identical to Dirac distributions and centered on the same value of θ. One WDF is the O mode, and the other the X mode.

It can be observed that the P' functions are generally more sensitive to large θ values. Region 1 of the CMA diagram is again the only one where electric as well as magnetic estimators can be used. For the case shown in Figure 5, panels A_1 and B_1, the electric and magnetic curves are quite similar, and P'_{EX} and P'_{HO} reach their maximum (≈ 0.2) at $\theta_E \simeq \theta_H \simeq 50°$, whereas P'_{EO} and P'_{HX} are monotonic functions that run from zero at $\theta = 0°$ to ∞ at $\theta = 90°$. $P'_{E(O+X)}$ and $P'_{H(O+X)}$ are mean curves varying from 0 to 1. Referring to the relations (11), we see that $P_E > 0.2$ indicates the presence of an O mode whereas $P_H > 0.2$ identifies the presence of an X mode. It is likely that the hypothesis of a single propagating mode can be made for P_E or $P_H \gg 0.2$. The main contribution to the final value of the P_E and P_H estimators is due to large θ waves, one possible definition of the large θ waves being $\theta > \theta_E$, θ_H. For the case shown in Figure 5, panels A_3 and B_3, the situation is almost the same for P_H, P'_{HO} having a maximum ≈ 0.2 at $\theta_H \simeq 52°$. Due to the logarithmic scale, the P'_{EX} curve is not represented, but a threshold < 0.01 may be adopted to point out the presence of the O mode (see Figure 11).

The situation in region 3 is illustrated in Figure 5, panel B_4. There is a resonance angle for the X mode at $\theta = 25°$. The maximum of the P'_{HO} curve is equal to ≈ 0.1 for $\theta_H \simeq 40°$. The two examples of region 6-a (panels B_2 and B_5) have slightly different maxima, but do not present any particularity.

Returning to (11), it can be concluded that P_E values greater than Q_E indicate the presence of the O mode. The exact P_E value depends on θ and on the wave energy density in each mode. In the same way, P_H values greater than Q_H correspond to the presence of the X mode. On the other hand, a value of P_E less than Q_E, or of P_H less than Q_H, cannot be readily interpreted since it may be due to parallel waves in any mode as well as to nonparallel waves in the X mode for P_E and in the O mode for P_H.

The Mode Identification

Combining the results obtained for the quasi-parallel and quasi-perpendicular estimators, one generally obtains good information on the propagation mode present in the medium and on their propagation characteristics, without any hypothesis on the θ distribution. This is illustrated in Figure 6 for two different values of the wave and plasma parameters. The symbols ($\parallel$) and ($\perp$) represent quasi-parallel and quasi-perpendicular propagation and are absent for propagation that is both parallel and perpendicular; θ_r is the resonance angle of the R-X mode at $f_{pe}/f = 0.75$ and $f_{ce}/f = 0.9$. We assume that in regions where they can be compared, there is no inconsistency between the signs of Im (S_{12}) and Im (S_{45}). Obviously, simultaneous values of P_E and P_H, such as
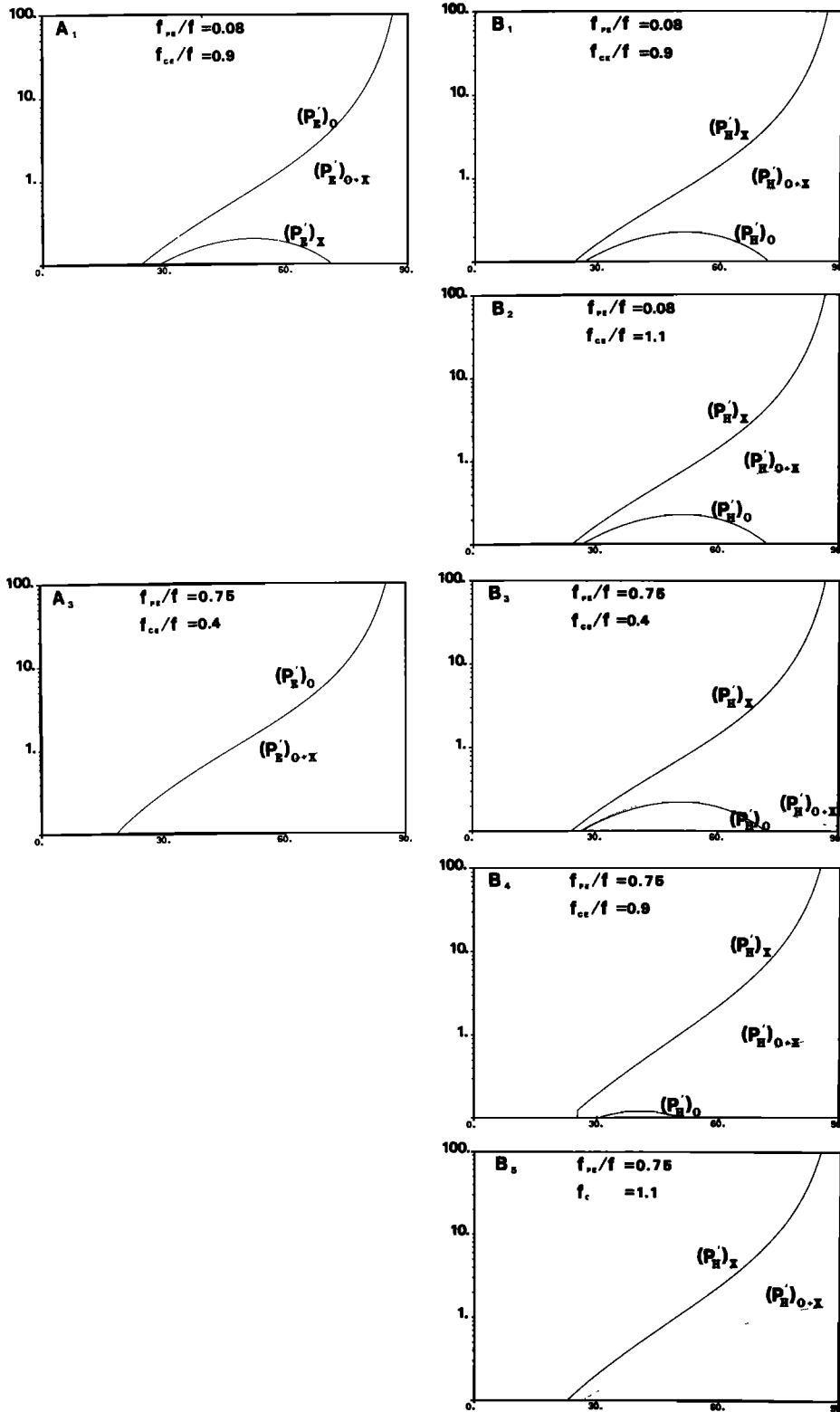
Fig. 5. Variations of $(P'_E)_X$, $(P'_E)_O$, $(P'_H)_X$, and $(P'_H)_O$ versus θ (solid line); $(P'_E)_{X+O}$ and $(P'_H)_{X+O}$ (dotted line). The plasma parameters are the same as in Figure 4.
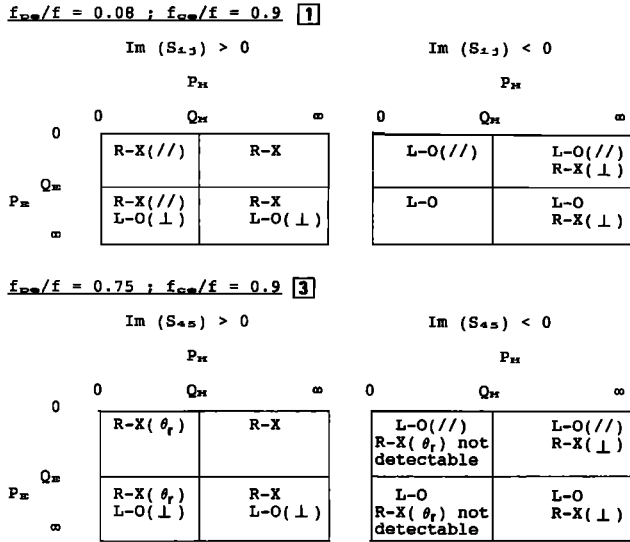
Fig. 6. Identification of the propagation modes and the main propagation characteristics when combining the quasi-parallel and quasi-perpendicular estimations of polarization. In the top panel, Im (S_{ij}) means either Im (S_{12}) or Im (S_{45}).

$P_E \gg Q_E$ and $P_H \gg Q_H$, correspond to cases with two modes.

All these considerations being taken into account, it is observed that, provided the WDFs in each mode have different θ distributions, one can make the distinction between propagations in a single mode or in two modes, with indications on the general propagation characteristics: quasi-parallel or quasi-perpendicular. There are exceptions in cases with a dominant mode, i.e., when there is a large difference in the value of the Im (a_{12m}) and Im (a_{45m}) coefficients. In such cases there will always exist combinations of the sign of Im (S_{12}) and Im (S_{45}), and of the value of P_E and P_H, for which it is impossible to see whether the nondominant mode is present or not. The case of a dominant mode is discussed further in section 3.

The technique can be applied to experimental data. Knowing the plasma parameters f_{ce} and f_{pe} and the wave frequency, one needs only to look to the sign of Im (S_{12}) and/or Im (S_{45}) and to calculate the ratios P_E and/or P_H. These ratios must be compared to thresholds evaluated as in (11). An example of the identification of the modes with synthetic data is given below.

Examples of Applications

As an example of application, consider five different models of WDF (see Figure 7) where waves in the R-X and in the L-O modes are simultaneously present. For the sake of simplicity, it is assumed that the WDF in each mode is constant over a given θ interval, the central θ values of the WDFs being different for the two modes. No information on the Φ distribution is needed since Im (a_{12m}) and Im (a_{45m}) are not Φ dependent. For each model, taking the plasma parameters of Figure 4, one obtains with (6) the values of Im $[S_{12}(f)]$ and Im $[S_{45}(f)]$. Then, applying (7) and (8), one estimates a propagation mode. The set of results is summarized in Table 2 a. In order to avoid too specific discussions, we have not considered the plasma parameters of Figure 4,

panel B_4, for which a resonance angle has to be taken into account.

The following two points come out:

1. For wave frequencies very close to a critical frequency ($f = f_X$ in panel B_3 of Figure 4) it is always the L-O mode which is identified, unless it has very little energy compared to the R-X mode, which is consistent with panel B_3 of Figure 4, where the Im (a_{45}) values in the R-X mode are always negligible in relation to the Im (a_{45}) values in the L-O mode.

2. There is no simple rule to determine which waves have the most important contribution to the signs of Im (S_{12}) and Im (S_{45}).

The only way to improve our mode identification is to compute the values of the P_E and P_H estimators and to compare them to the Q_E and Q_H thresholds. This has been done for the same conditions as above, substituting the five WDF models into (6). The Q_E and Q_H values are directly derived from Figure 5. The set of all relevant values is given in Table 2b. The results of the tests are summarized in Table 2c. The dashes mean that $P_E < Q_E$ or $P_H < Q_H$. We note that (1) in most cases, P_E and P_H values of the order of 0.2 are high enough to detect the presence of a given mode, and (2) as forecast, P_E values are used to point out the presence of one mode (here L-O) whereas P_H values are used to point out the presence of the other mode (here R-X), the two measurements being sometimes complementary (model 5).

Now, examining Tables 2 a and 2 c, we see that in most cases where electric and magnetic measurements can be compared (A_1 and B_1, A_3 and B_3) one identifies the simul-
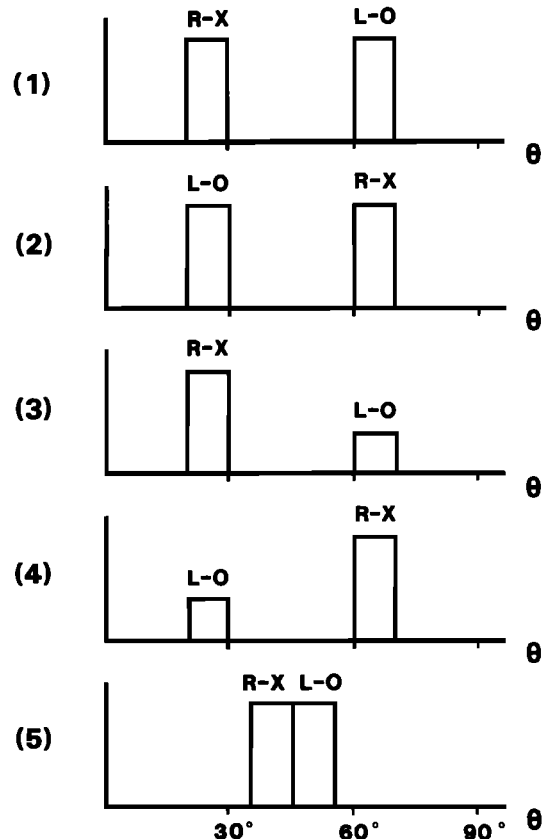

Fig. 7. Models of WDF used for a test on synthetic data. The units are arbitrary.

TABLE 2a. Results of the Test With Synthetic Data Obtained From Figure 7: Polarization Estimator for Quasi-Parallel Waves

Model	Region 1, Case A1	Region 1, Case A3	Region 1, Case B1	Region 6a, Case B2	Region 1, Case B3	Region 6a, Case B5
1	R-X	R-X	R-X	R-X	L-O	R-X
2	L-O	L-O	L-O	L-O	L-O	L-O
3	R-X	R-X	R-X	R-X	L-O	R-X
4	R-X	R-X	L-O	R-X	L-O	L-O
5	L-O	R-X	L-O	L-O	L-O	L-O

The first two columns refer to panels A_1 and A_3 of Figure 4 obtained for electric measurements, whereas the last four refer to panels B_1 to B_5 of Figure 4, obtained for magnetic measurements.

taneous presence of the two modes. In all the other cases, where we rely on the magnetic data only, the full identification depends on the sign of Im (S_{45}). If it is negative, i.e., if it shows up the L-O mode, the P_H estimator may point out the presence of the R-X mode. If it is positive, i.e., if it corresponds to the R-X mode, it is not necessary to estimate the P_H value any more: it does not contain any supplementary information.

Returning to the ideal cases where magnetic plus electric data may be compared, most of the time one can obtain first approximations on the propagation characteristics in each mode. As an example, consider plasma parameters of panels A_1 and B_1 of Figures 4 and 5. Applying the strategy defined in Figure 6 and using the signs of Im (S_{ij}) and the P_E, P_H values of Table 2, one observes that for model 1, the R-X mode is conveyed by rather parallel waves and the L-O mode by rather perpendicular waves; model 2 is the opposite of model 1; the propagation characteristics of model 3 are similar to those of model 1; the L-O mode of model 4 is not detected; and finally for model 5 we find L-O mode waves plus R-X mode waves propagating with K vectors nearly perpendicular to B_0.

An experimental illustration of the interest of a good definition of the P_E threshold can be found in the Viking data recorded by the V4H experiment [Bahnsen et al., 1987]. In this experiment, the measured electric field component is alternatively almost parallel, then perpendicular to the geomagnetic field B_0. Then, assuming the wave field is time stationary, after half the spin rotation one may estimate P_E (see equation (9)). This has been done for the event of Figure 1 of de Feraudy et al. [1987] just at the time ($\simeq$2033 UT) where the satellite seems to pass through the source region of AKR emissions. Assuming that the plasma frequency is given by the upper cutoff frequency of the VLF hiss [de

Feraudy et al., 1987] we obtain $f_{pe} = 20$. kHz. As $f_{ce} = 208$ kHz, when working at $f = 233$ kHz, we have $f_{pe}/f = 0.085$ and $f_{ce}/f = 0.89$, which is typically the case of our Figure 5, panel A_1. The computation of P_E gives $P_E = 1.12$. Referring to Figure 5, panel A_1, and equation (12), P_E is compared against $Q_E = 0.20$. Our conclusion is that, as suggested by de Feraudy et al. [1987], L-O mode waves are definitely present. Moreover, if we take the lower cutoff frequency of the event as well as the spin modulation pattern of the band as indicators of the presence of R-X mode waves, we find, with de Feraudy et al., that AKR emissions in the source regions are the sum of L-O and R-X mode waves. However, to be affirmative about the presence of R-X mode waves, one would need to estimate the quantities (7), (8), and (9).

3. THE VALIDITY DOMAINS

The Dominant Modes

To determine the wave and plasma parameters for which the quasi-parallel polarization estimators are strongly biased toward one of the two modes (see Figure 4, panel B_3), we define the quantities

$$R_{12} = \frac{\text{Im } [a_{12}(\theta)]_L}{\text{Im } [a_{12}(\theta)]_R}$$

$$R_{45} = \frac{\text{Im } [a_{45}(\theta)]_L}{\text{Im } [a_{45}(\theta)]_R}$$

(12)

For R_{12} and R_{45} greater than 1 the L mode is called the dominant mode, while for R_{12} and R_{45} less than 1 the R mode is dominant. When one mode is dominant, the polarization

TABLE 2b. Results of the Test With Synthetic Data Obtained From Figure 7: Polarization Estimator for Quasi-Perpendicular Waves

Model	Case A1, $Q \simeq 0.22$	Case A3, $Q \simeq 10^{-3}$	Case B1, $Q \simeq 0.22$	Case B2, $Q \simeq 0.12$	Case B3, $Q \simeq 0.21$	Case B5, $Q \simeq 0.10$
	P_E	P_E	P_H	P_H	P_H	P_H
1	0.70	0.81	0.14	0.12	0.16	0.06
2	0.13	0.11	0.54	0.59	0.14	0.64
3	0.38	0.37	0.12	0.11	0.15	0.08
4	0.13	0.06	0.94	1.05	0.23	1.23
5	0.33	0.39	0.32	0.32	0.23	0.30

The column heads refer to panels of Figure 5.

TABLE 2c.   Results of the Test With Synthetic Data Obtained from Figure 7: Polarization
Estimator for Quasi-Perpendicular Waves

Model	Case A1	Case A3	Case B1	Case B2	Case B3	Case B5
1	L-O	L-O	···	···	···	···
2	···	L-O	R-X	R-X	···	R-X
3	L-O	L-O	···	···	···	···
4	···	L-O	R-X	R-X	R-X	R-X
5	L-O	L-O	R-X	R-X	R-X	R-X

The column heads refer to panels of Figure 5.

estimators tend to favor this mode although the other mode may be of larger energy density, thereby rendering the mode identification difficult.

In order to study the behavior of R_{12} and R_{45} for different regions of the CMA diagram, the f_{pe}/f ratio was fixed, and the f_{ce}/f ratio was taken as variable. Three f_{pe}/f values are considered: 0.08 (the left vertical line in Figure 2 a), 0.75 (the middle vertical line), and 1.2 (the right vertical line).

To have an idea of the θ dependence, the computations of R_{12} and R_{45} are done for one large θ value (solid curve) and for one small θ value (dashed line). Generally one takes θ = 80° and θ = 5°, respectively, but those values may be modified in regions with either a resonance angle θ_r or an angle θ_c for which $n^2 = S$. The R_{12} quantity was estimated even within regions of the CMA diagram where the identification of the propagation modes is impossible from the electric measurements.

Figure 8a shows the variation of R_{12} as a function of f_{ce}/f for f_{pe}/f = 0.08. For $R_{12} > 1$, there is a tendency to observe the left-handed polarized mode, even if the right-handed polarized mode has the same wave energy density; for $R_{12} < 1$ the tendency is to observe the right-handed mode. As f_{ce}/f increases, one passes from region 1 in the CMA diagram to region 6 (regions 2 and 3 are not seen in the graph due to the f_{pe}/f value and the frequency bin). In region 1 there is an equal contribution of the two modes for $f_{ce}/f < 0.3$. When f_{ce}/f approaches 1, large θ waves have a higher contribution in the R-X mode than in the L-O mode, whereas low θ waves show a higher contribution in the L-O mode close to f_{ce}/f = 1 only. When $f < f_{ce}$, the L-O mode is greater than the Z right-handed mode, particularly for the large θ waves. Note that for f_{ce}/f values between 1.0 and 1.123, the quantity $n^2 - S$ is negative at θ = 80°, which means that no mode identification is possible, at least from the electric measurements. Figure 8b concerns the magnetic measurements (R_{45}). The θ = 5° and θ = 80° solutions are practically identical, except in a very narrow domain around $f = f_{ce}$ where the L-O mode is dominant above f_{ce} as well as below.

More important effects are seen for f_{pe}/f = 0.75 (Figure 9). When the electric measurements are considered (Figure 9a), no mode identification is possible between the R = 0 cutoff (f_X frequency) and the electron gyrofrequency with our method. This poses no problem for the interval between f_X and f_{UHR} (region 2 of the CMA diagram) since only one single mode propagates here. However, the interval between f_{UHR} and f_{ce} corresponds to region 3, for which the interpretation of the sign of Im (S_{12}) is ambiguous. For $f_{ce}/f > 1$, in region 6-a, the mode identification is again not possible up to a f_{ce}/f value given by θ (see Figure 3). The latter constraint explains why there is no θ = 80° curve below f_{ce} on the present graph. In any case, the interpretation of the sign of

Im (S_{12}) in this region of the CMA diagram is generally impossible since one does not know beforehand the position of the distribution in θ, with respect to the θ_c angle. For $f_{ce}/f < 1$, it is the mode with the highest wave energy that gives the sign of Im (S_{12}) if the waves propagate with small θ values. But as soon as large θ waves are present in the R-X mode (for instance, $\theta > 30°$ at f_{ce}/f = 0.4 in Figure 4, panel B3), they control the sign of Im (S_{12}).

The mode identification is easier with magnetic measurements (Figure 9b). The L-O mode is dominant below f_{ce}/f_X, the small θ values being more sensitive to this mode. Above f_{ce}/f_{UHR} the frequency domain for which the R_{45} curves may be drawn is a function of the θ value under consideration. It starts from the vicinity of f_{ce}/f_{UHR} for a large θ value, but from $f_{ce}/f \simeq 1$ for small θ values. Although the interpretation is difficult, it is clear that at f_{ce}/f values below $\simeq 1.5$ the L-O mode is dominant, whereas above this value it is the R-X
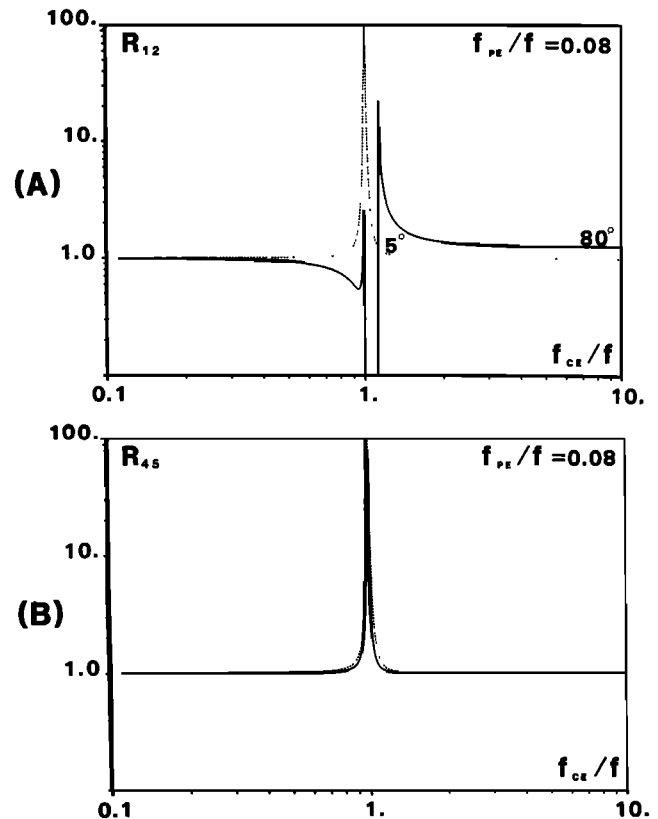

Fig. 8.   (a) Ratio between Im (a_{12}) in the L mode and Im (a_{12}) in the R mode as a function of f_{ce}/f, with f_{pe}/f = 0.08, f = 300 kHz. The solid line corresponds to θ = 80°, and the dashed line to θ = 5°. (b) Same as Figure 8a, but for Im (a_{45}).

mode. For f_{ce}/f values in between f_{ce}/f_{UHR} and 1.0, there is no propagation of small θ waves due to the resonance angle.

At $f_{pe}/f = 1.2$ (Figure 10), a mode identification is required for $f_{ce}/f > 1$ only (region 7). Due to the existence of a resonance angle the large θ value has been fixed at 20°. The solutions obtained for the electric measurements are displayed in Figure 10a. The left-handed polarized mode (Z mode here) is dominant over a large frequency domain. As far as the solutions obtained for the magnetic measurements are concerned (Figure 10b), they favor the Z mode just below f_{ce}. At smaller frequencies, the Z mode is very slightly dominant for the largest θ waves (which here are very small), whereas it is the whistler mode for the smallest θ waves.

The P_E and P_H Thresholds

The variations of the P'_{EX} and P'_{HO} maximum values denoted Q_E and Q_H, respectively, as regards f_{ce}/f, are shown in Figure 11 for $f_{pe}/f = 0.08$ (A$_1$, B$_1$), 0.75 (A$_2$, B$_2$), and 1.2 (A$_3$, B$_3$). Note that the Q_E values have not been plotted in regions where the tests on the parallel to perpendicular energy of the electric field are not relevant. So one can consider that in the present field of study, electric and magnetic thresholds are always below ≈ 0.6. At fixed f_{pe}/f values, they both decrease when f_{ce}/f increases, and, conversely, at fixed f_{ce}/f value they both decrease when f_{pe}/f increases.

In any case, one is very far from the constraints when assuming plane waves at $\theta = 90°$ ($P_E \rightarrow \infty$ for the O mode and $P_H \rightarrow \infty$ for the X mode). Values of P_E and P_H greater than
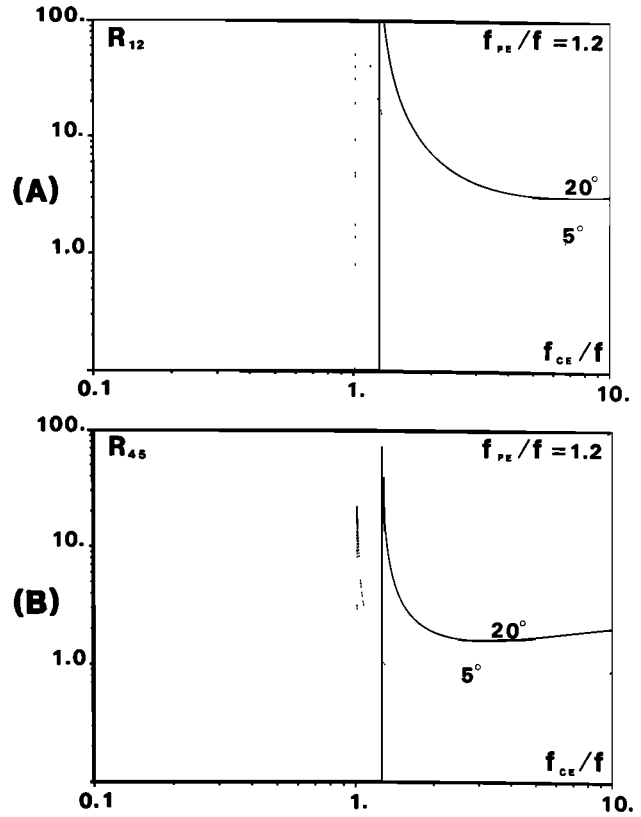

Fig. 10. (a) Same as Figure 8a but for $f_{pe}/f = 1.2$. The solid line corresponds to $\theta = 20°$, and the dashed line to $\theta = 5°$. (b) Same as Figure 10a but for Im (a_{45}).

a fraction of unity are sufficient to point out the presence of waves propagating in O or X modes.

As an indication, Figure 12 shows the variations of the θ_E and θ_H angles; θ_E values have not been plotted in regions where the polarization of the electric field is not readily interpretable. We see that the waves that contribute the most to the P_E and P_H values always have θ values above 70° for the magnetic measurements but they can also include waves propagating at $\theta \simeq 20°$ for the electric measurements ($f_{pe}/f = 1.2$). The electric measurements, which were already found to provide a poor estimator of the polarization of quasi-parallel waves (see previous section), may also give rise to a poor estimator of the polarization of quasi-perpendicular waves.

4. CONCLUSION

We have studied the problem of interpreting the direct measurements of polarization sense for HF plasma waves in a cold and collisionless magnetoplasma, in the case where two magnetoionic modes may simultaneously be present. It is shown that two types of propagation estimators could be considered.

The first estimator, generally more sensitive to the quasi-parallel waves, consists in the determination of the signs of Im (S_{12}) and Im (S_{45}): the imaginary parts of measured cross-spectra between two electric or two magnetic wave field components, both perpendicular to each other and to the Earth magnetic field. According to the wave and plasma parameters at the point of measurement the estimator may be more sensitive to one mode than to the other. The
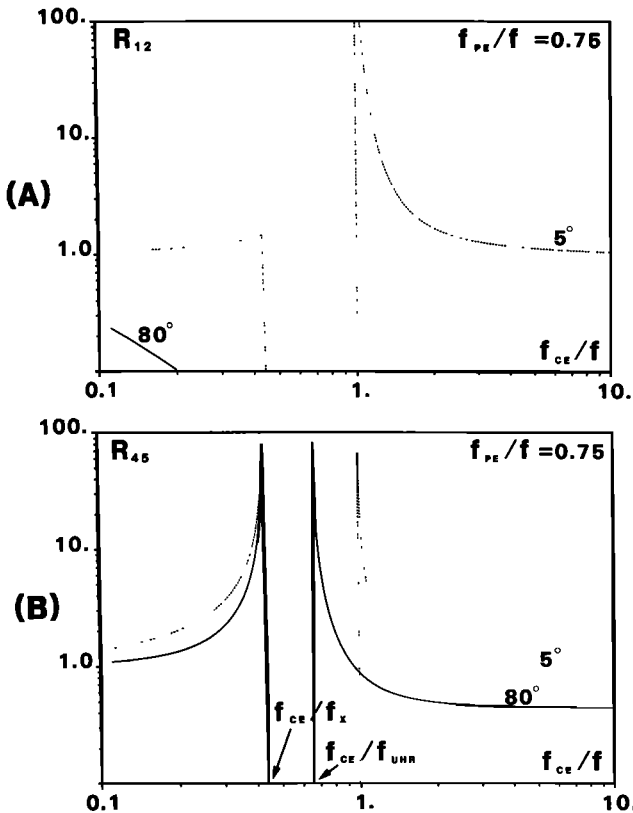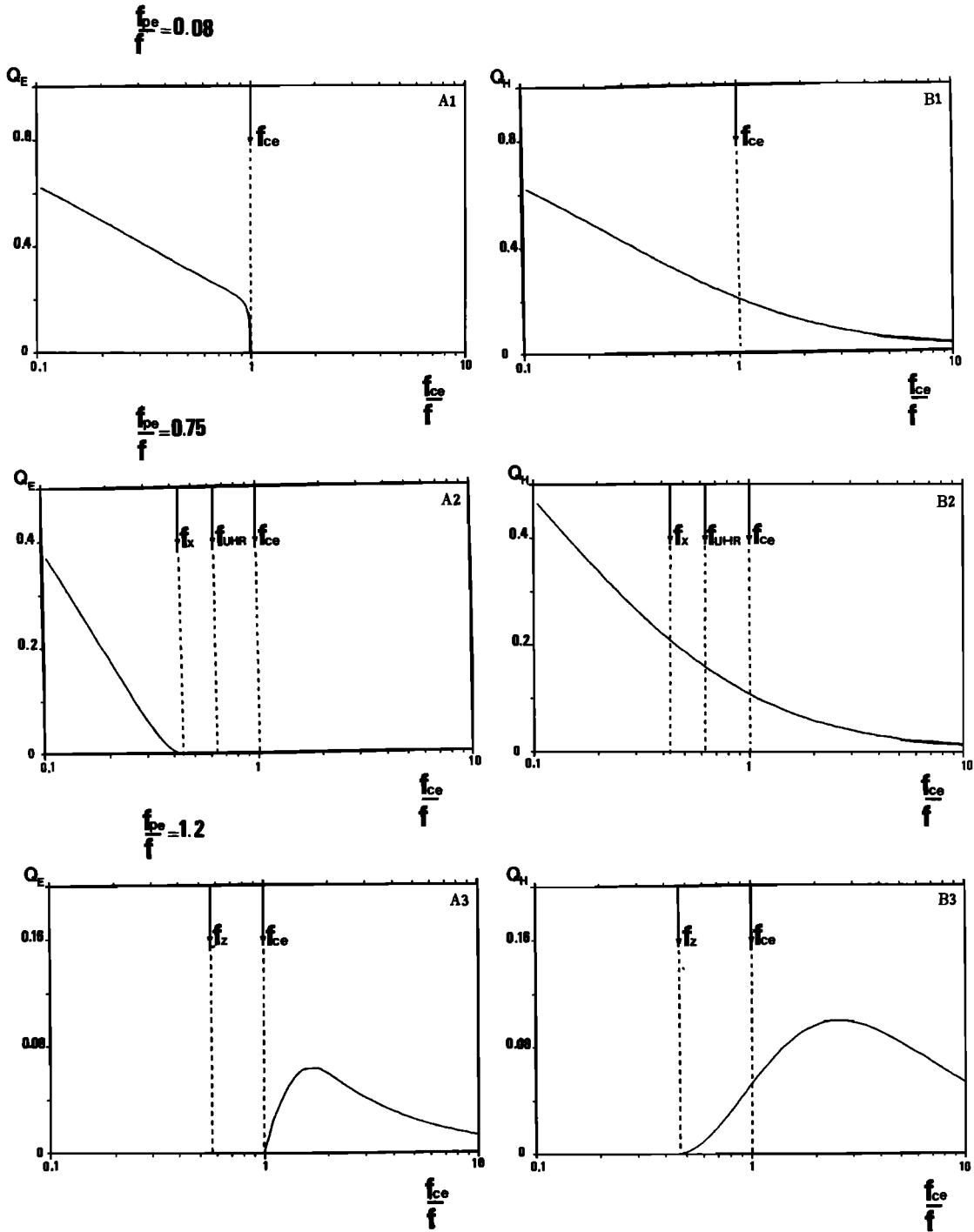

Fig. 9. (a) Same as Figure 8b but for $f_{pe}/f = 0.75$. The solid line corresponds to $\theta = 80°$, and the dashed line to $\theta = 5°$. (b) Same as Figure 8b but for $f_{pe}/f = 0.75$.

$\dfrac{f_{pe}}{f} = 0.08$

$\dfrac{f_{pe}}{f} = 0.75$

$\dfrac{f_{pe}}{f} = 1.2$

Fig. 11.   Variations of Q_E and Q_H versus f_{ce}/f for $f_{pe}/f = 0.08$ (A$_1$, B$_1$), $f_{pe}/f = 0.75$ (A$_2$, B$_2$), and $f_{pe}/f = 1.2$ (A$_3$, B$_3$).
The wave frequency is $f = 300$ kHz.

phenomenon may be so important at the vicinity of the characteristic frequencies of the medium (electron gyrofrequency, upper hybrid frequency, $R = 0$ cutoff frequency, etc.) that the identification of a given mode may be impossible, even when it conveys the largest wave energy density. The estimator used for the electric measurements (Im (S_{12})) presents two serious drawbacks: first, it does not apply in specific regions of the CMA diagram, and second, it may be sensitive to quasi-perpendicular waves. There is no restriction for the estimator used for the magnetic measurements (Im (S_{45})).

The second estimator, more sensitive to the quasi-perpendicular waves, is obtained by testing the values P_E and P_H of the ratio of the parallel to the perpendicular energy, in the electric and magnetic wave field components, against thresholds. A major result of the study is the definition of thresholds for electric as well as for magnetic measurements. Their values, which depend on the wave and plasma parameters, are always much lower than 1. For instance, with the parameters used for Figures 4 and 5, P_E and P_H values greater than 0.2 are sufficient to establish the existence of O and X polarization, respectively. Infinite (or large) values of P_E and
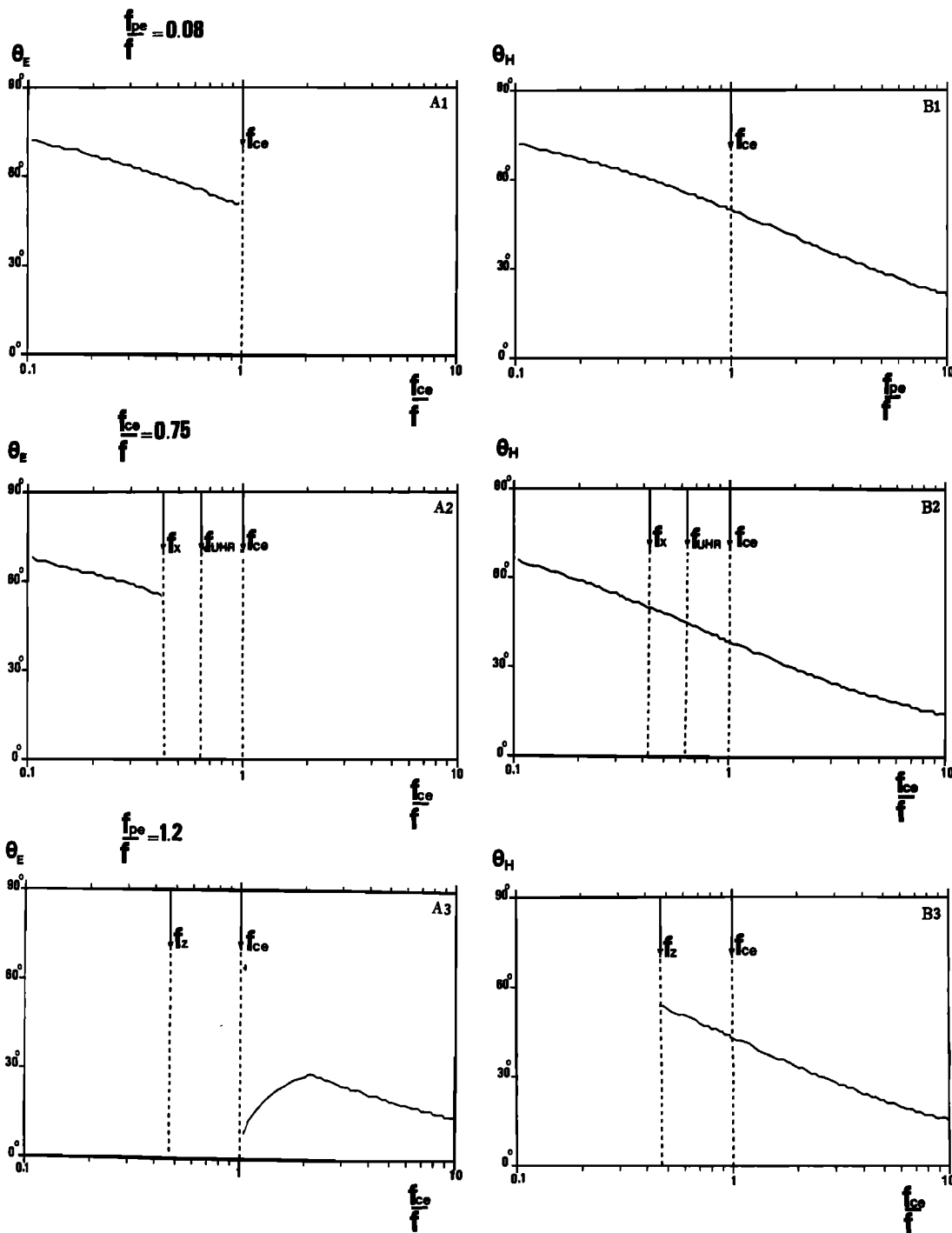
Fig. 12.   Variations of θ_E and θ_H versus f_{ce}/f for f_{pe}/f = 0.08 (A$_1$, B$_1$), 0.75 (A$_2$, B$_2$), and 1.2 (A$_3$, B$_3$). The wave frequency is f = 300 kHz.

P_H are not required. An example of application to Viking data has enabled us to check that in the source region, AKR emissions could be the sum of L-O and R-X waves.

Applications have been performed on synthetic data constructed from two-propagation mode models with different wave distribution functions. They show that the combination of the four estimators often enables us to point out the simultaneous presence of the two modes. Moreover, when the WDFs of the two modes are very different and when the wave frequency is far from the characteristic frequency of the medium, the main propagation characteristics in each

mode (propagation quasi-parallel or quasi-perpendicular) may be derived. But obviously there are cases where the use of the propagation mode estimators does not lead to reliable identifications. The only way to proceed is to perform a full determination of the WDFs in each mode, which has never been undertaken so far. As a consequence, if one wants to avoid any misinterpretations, one must carefully study the properties of the propagation mode estimators—as we did— with the wave and plasma parameters in hand, before starting the analysis of real data.

As long as the waveforms of the electric and magnetic

wave field components of HF waves are not simultaneously recorded before being transmitted to the ground, it will not be possible to fully apply the techniques proposed here to real data. However, this will become possible in the near future with the Soviet Interball project.

APPENDIX

Here we give expressions of the kernels a_{ij} used in this paper, as a function of the plasma parameters.

$$\text{Im } (a_{12}) = \frac{(n^2 - P)^2}{n^4(n^2 - L)^2} (n^2 - S)D\chi$$

$$\text{Im } (a_{45}) = \frac{(n^2 - P)^2 \cos^2 \theta}{n^2(n^2 - L)^2} (n^2 - S)D \frac{P}{P - n^2 \sin^2 \theta} \chi$$

$$a_{33} = \frac{(n^2 - R)^2 \cot^2 \theta}{n^4} \chi$$

$$a_{11} + a_{22} = \frac{(n^2 - P)^2(n^2 - R)^2}{2n^4} \left\{ \frac{1}{(n^2 - R)^2} + \frac{1}{(n^2 - L)^2} \right\} \chi$$

$$a_{66} = \frac{(n^2 - P)^2(R - L)^2 \sin^2 \theta}{4n^2(n^2 - L)^2} \chi$$

$$a_{44} + a_{55} = \frac{\cos^2 \theta}{2n^2(n^2 - L)^2}$$

$$\cdot \{(P - L)^2(n^2 - R)^2 + (P - R)^2(n^2 - L)^2\}\chi$$

with

$$\chi = 8[\varepsilon_0 \nu_g(\lambda' + \mu')]^{-1}$$

$$\lambda' = 2(P - R)^2 \left\{ 1 + \frac{(P - L)^2(n^2 - R)^2}{(P - R)^2(n^2 - L)^2} \right\} \cos^2 \theta$$

$$\mu' = \frac{(R - L)^2(n^2 - P)^2}{(n^2 - L)^2} \sin^2 \theta$$

$$\nu_g = \frac{1}{2}\omega^3 \frac{\delta}{\delta\omega}[-(\omega n)^{-2}]$$

REFERENCES

Allis, W. P., S. J. Buchsbaum, and A. Bers, *Waves in Anisotropic Plasmas*, MIT Press, Cambridge, Mass., 1963.

Bahnsen, A., M. Jespersen, E. Ungstrup, and I. B. Iversen, Auroral hiss and kilometric radiation measured from the Viking satellite, *Geophys. Res. Lett.*, *14*, 471, 1987.

Benson, R. F., Ordinary mode auroral kilometric radiation, with harmonics, observed by ISIS 1, *Radio Sci.*, *19*, 543, 1984.

Benson, R. F., and W. Calvert, ISIS 1 observations at the source of auroral kilometric radiation, *Geophys. Res. Lett.*, *6*, 479, 1979.

de Feraudy, H., B. M. Pedersen, A. Bahnsen, and M. Jespersen, Viking observations of auroral kilometric radiation from the plasmasphere to night auroral oval source regions, *Geophys. Res. Lett.*, *14*, 511, 1987.

Grabbe, C. L., Auroral kilometric radiation: A theoretical review, *Rev. Geophys.*, *19*, 627, 1981.

Gurnett, D. A., and J. L. Green, On the polarization and origin of auroral kilometric radiation, *J. Geophys. Res.*, *83*, 689, 1978.

Gurnett, D. A., S. D. Shawhan, and R. R. Shaw, Auroral hiss, Z mode radiation, and auroral kilometric radiation in the polar magnetosphere: DE 1 observations, *J. Geophys. Res.*, *88*, 329, 1983.

Kaiser, M. L., J. K. Alexander, A. C. Riddle, J. B. Pearce, and J. W. Warwick, Direct measurements by Voyager 1 and 2 of the polarization of terrestrial kilometric radiation, *Geophys. Res. Lett.*, *5*, 857, 1978.

Lefeuvre, F., Y. Marouan, M. Parrot, and J. L. Rauch, Rapid determination of the sense of polarization and propagation for random electromagnetic wave fields. Application to GEOS-1 and AUREOL-3 data, *Ann. Geophys.*, *Ser. A*, *4*, 457, 1986. (Correction, *Ann. Geophys.*, *Ser. A*, *5*, 251, 1987.)

Marouan, Y., Etats de polarisation et détermination des caractéristiques moyennes des ondes naturelles dans un magnétoplasma froid. Application à des données EBF, Ph.D. thesis, Univ. Orléans, Orléans, France, 1988.

Oya, H., and A. Morioka, Observational evidence of Z and L-O mode waves as the origin of auroral kilometric radiation from the Jikiken (EXOS-B) satellite, *J. Geophys. Res.*, *88*, 6189, 1983.

Shawhan, S. D., and D. A. Gurnett, Polarization measurements of auroral kilometric radiation by Dynamics Explorer-1, *Geophys. Res. Lett.*, *9*, 913, 1982.

Stix, T. H., *The Theory of Plasma Waves*, McGraw-Hill, New York, 1962.

Storey, L. R. O., and F. Lefeuvre, The analysis of 6-component measurements of a random electromagnetic wave field in a magnetoplasma, I, The direct problem, *Geophys. J. R. Astron. Soc.*, *56*, 255, 1979.

Storey, L. R. O., and F. Lefeuvre, The analysis of 6-component measurements of a random electromagnetic wave field in a magnetoplasma, II, The integration kernels, *Geophys. J. R. Astron. Soc.*, *62*, 173, 1980.

F. Lefeuvre, Y. Marouan, and M. Parrot, LPCE/CNRS, 3A, Avenue de la Recherche Scientifique, 45071 Orléans Cedex 02, France.